A comparative DFT assessment of the mechanical, elastic, electronic, and optical parametric study of perovskites $CsPbX_3$ for opto-electronic applications

S. M. Junaid Zaidi[a], M. Sana Ullah Sahar[b], M. Ijaz Khan[c,*], Hafiz T. Ali[d], M. Khalid[e], M. Shahid[f]

[a]*Department of Physics and Mathematics, Faculty of Sciences, Superior University, Lahore – 54000, Pakistan*

[b]*Department of Mechanical, Industrial, and Energy Systems, University of Sargodha, Sargodha – 40100, Pakistan*

[c]*Institute of Mechanical and Manufacturing Engineering, Khwaja Fareed UEIT, Rahim Yar Khan, Pakistan*

[d] *Department of Mechanical Engineering, College of Engineering, Taif University, Kingdom of Saudi Arabia.*

[e]*School of Chemical Engineering and Technology, Xi'an Jiaotong University, Xi'an - 710049, China*

[d]*Institute of Mechanics of Materials, Ruhr-Universität Bochum, Universität Str. 150, 44801, Bochum, Germany*

Perovskites, specifically $CsPbX_3$ (X= F, Cl, Br, I), are gaining attention for their remarkable optoelectronic features, suitable for applications like solar cells, LEDs, and photodetectors. Utilizing Density Functional Theory (DFT), this study explores $CsPbX_3$'s electronic, mechanical, and optical properties. $CsPbI_3$ and $CsPbBr_3$ exhibit ideal electronic traits with a large band gap and excellent optical features, making them optimal for solar cells and LEDs. $CsPbF_3$ stands out for superior mechanical properties, ideal for applications like scintillators. Overall, $CsPbI_3$ and $CsPbBr_3$ excel in electronic and optical aspects, while $CsPbF_3$ is mechanically robust.

(Received January 12, 2024; Accepted August 14, 2024)

Keywords: DFT, Density of states, Optical properties, Elastic properties

1. Introduction

Perovskites are a category of materials that share a particular crystal structure with the mineral perovskite, it has the general formula ABX_3 and contains the cations A and B together with the anion X [1]– [5]. Due to their potential use in a variety of technologies, such as solar cells [6]– [9], light emitting diodes LEDs [10], lasers [11], photodetectors [12], energy storage devices [13] and sensing devices [14] perovskites have gained a lot of attention recently. Particularly perovskite solar cells have seen amazing efficiency advancements and have the potential to replace conventional silicon-based solar cells as a low-cost and effective option [15]. Materials made of perovskite have certain characteristics that render them perfect for these uses [16]. They can absorb a lot of light with a relatively little layer of material due to their high absorption coefficient [17]. Moreover, they are adaptable for a variety of applications due to their high charge carrier mobility [18], which facilitates rapid charge transfer[19], and the ability to control their band gap by altering the material's composition [20]. The high-power conversion efficiencies and inexpensive manufacturing methods of perovskite solar cells have helped them quickly establish themselves as one of the most promising next-generation solar technologies [21].

Depending on the exact application and device architecture, the optimal bandgap for perovskite solar cell production typically falls between 1.5 and 1.7 eV. A perovskite absorber layer is often placed between two charge-selective layers in perovskite solar cells. The range of light wavelengths that can be effectively absorbed and converted into power is determined by the

* Corresponding author: ijazkhan4123@gmail.com
https://doi.org/10.15251/DJNB.2024.193.1227

bandgap of the perovskite absorber layer. A band gap that is too big could lead to decreased photocurrent, while a bandgap that is too narrow could cause thermalization losses and decreased efficiency [8], [22]–[24]. The highest power conversion efficiencies may be attained by perovskite solar cells with some record-breaking devices exceeding 25% efficiency, according to research. However, additional elements like charge transfer, recombination, and stability all have a significant impact on the overall effectiveness and dependability of perovskite solar cells [25], [26]. For a good solar cell the required optical parameters are high optical absorption in the solar spectrum (400–1100 nm) [27], high dielectric constant and low dielectric loss [28], energy loss function less than 0.1 eV [29], reflectivity less than 10% across the solar spectrum [30] and the refractive index greater than 2 [23].

Scintillators have demonstrated potential scope in X-ray detection. High optical absorption in perovskite scintillators is necessary for the effective conversion of incoming radiation into scintillation light. High reflectivity can cause scintillation light to be lost, which lowers the overall efficiency and energy resolution of scintillation. A high dielectric constant can have an impact on the scintillator's ability to gather light, collect light, and resolve energy. Low dielectric loss improves scintillation efficiency and reduces energy losses from dielectric heating. To achieve high energy resolution and scintillation efficiency, lower energy loss is preferred. For the best efficiency in light collecting and detection, the refractive index of the perovskite scintillator should match that of the other components of the scintillation detector, such as photodetectors and optical interfaces [31]–[36].

Perovskite LEDs (light-emitting diodes) can have different optical absorption, reflectivity, dielectric constant, energy loss, and refractive index needs depending on the precise composition and design of the perovskite material as well as the intended application of the LED. High optical absorption in the visible or near-infrared is often needed for perovskite LEDs. This guarantees effective electrical energy input absorption and effective light emission creation. By decreasing the amount of light lost through reflection at the surfaces, high reflectivity can aid in boosting the efficiency of the LED. Perovskite materials' dielectric properties, such as their dielectric constant and dielectric loss, can have an impact on how well they operate as LEDs. Low dielectric loss reduces energy losses from dielectric heating, however high dielectric constant might aid in limiting the electric field within the device, boosting charge injection and transport. Depending on the perovskite composition, layer thickness, and device architecture, the precise dielectric requirements could change. Dielectric heating reduces energy losses when there is low dielectric loss. To achieve high quantum efficiency, as well as efficient light emission, in the LED, lower energy loss is preferred [37]–[40].

There are several general requirements for a perovskite photodetector, such as having strong optical absorption in the desired wavelength range for the application. This guarantees effective absorption of the incident light, resulting in a high photodiode response and sensitivity. To maximize light absorption and raise photodiode efficiency, low reflectivity is typically preferred. For the photodiode to have high quantum efficiency and sensitivity, lower energy loss is preferred. Improved absorption and collection efficiency can be attained by using materials with higher refractive indices to confine and direct incident light inside the device [41]–[48]. The electronic, optical, mechanical, and elastic properties of the inorganic halide perovskites $CsPbX_3$ (X = F, Cl, Br, I) were investigated in this work using density functional theory in order to determine optimal mechanical, electronic, optical, and other parameters for use in optoelectronic devices such as light emitting diodes, solar cells, scintillators, photodiodes.

2. Methodology

$CsPbX_3$ (X = F, Cl, Br, I) have a cubic crystalline structure of space group pm-3m (221). The results of the structural, mechanical, electrical, optical, and photocatalytic features were compared and analyzed using DFT calculations using the CASTEP code in the Materials Studio simulation program [49]–[51]. Electrostatic interactions between component atoms' valance shells and ion cores were studied using the Generalized Gradient Approximation (GGA) of Perdew-Burke-Ernzerhof (PBE) and a norm-conserving pseudopotentials approach [52]–[55]. In contrast,

ultrasonic pseudopotentials were applied to estimate the mechanical characteristics to better match the experimental results. The Kohn-Sham equations were utilized for the computer simulations [56]–[58].

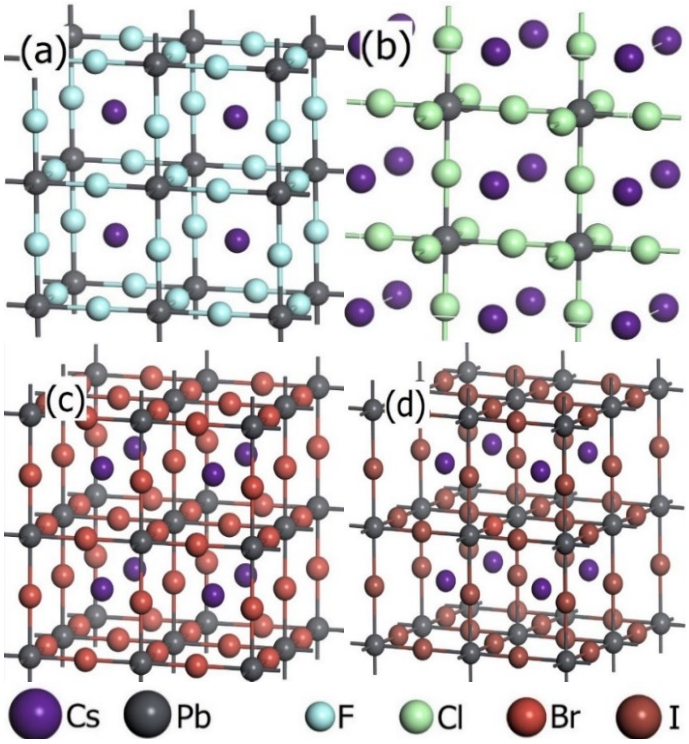

Fig. 1. Supercell cubic structures (a) $CsPbF_3$ (b) $CsPbCl_3$ (c) $CsPbBr_3$ (d) $CsPbI_3$.

As depicted in Fig. 1(b), the primitive cell of $CsPbCl_3$ consists of five atoms, with one "Cs" atom having site (0, 0, 0), three atoms of "Pb" at (0.5, 0.5, 0.5), and atom of Cl atom at (0.5, 0.5, 0.5) site. With a band energy tolerance of $1x10^{-5}$ eV in all cases, the cut-off energy of 400 eV for the plane-wave basis was set on plane-wave basic set points of $6 \times 6 \times 6$ k-points. The valence shell electronic configurations of Cesium (Cs), Lead (Pb), Fluorine (F), Chlorine (Cl), Bromine (Br), and Iodine (I) atoms are Cs: ($6s^1$), Pb: ($6s^2$, $4f^{14}$, $5d^{10}$, $6p^2$), F: ($2s^2$, $2p^5$), Cl: ($3s^2$, $3p^5$), Br: ($4s^2$, $3d^{10}$, $4p^5$), I: ($4d^{10}$, $5s^2$, $5p^5$).

3. Results and discussion

3.1. Lattice parameters calculations

According to simulation findings, the lattice parameters of cubic $CsPbF_3$, $CsPbCl_3$, $CsPbBr_3$, and $CsPbI_3$ are 4.973, 5.866, 6.138, and 6.515 Å respectively. The estimated volumes are similarly discovered to be 123.031, 201.914, 231.21 and 276.605 $Å^3$. $CsPbF_3$ has the lowest lattice parameter and unit cell volume values, whereas $CsPbI_3$ has the greatest values. From the lowest to the highest value, a relation may be stated as $CsPbF_3 < CsPbCl_3 < CsPbBr_3 < CsPbI_3$ for lattice parameters and volume outcomes of the $CsPbX_3$. The percentage increase in lattice parameters from $CsPbF_3$ was found at 17.9 %, 23.4 %, and 31.0 % for $CsPbCl_3$, $CsPbBr_3$, and $CsPbI_3$ respectively. Similarly, the increase in volume was found to be 64.1%, 87.9%, and 124% respectively.

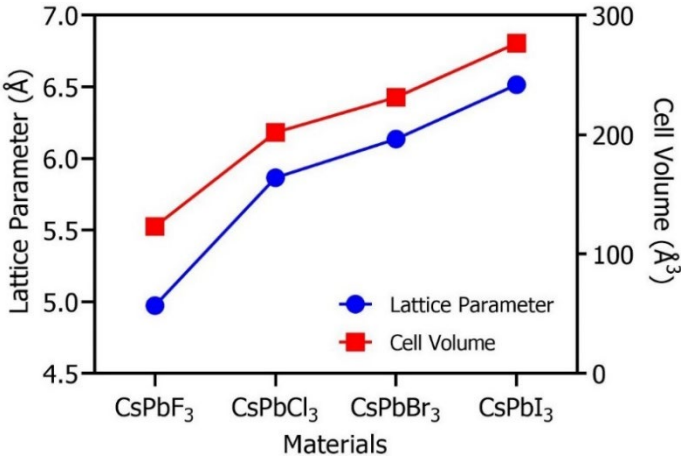

Fig. 2. The lattice parameters of the unit cell of $CsPbF_3$, $CsPbCl_3$, $CsPbBr_3$, and $CsPbI_3$, and their volume.

Table 1. Matching of lattice parameters and band gap of $CsPbX_3$ with other reported literature.

Material	Method	Lattice Parameter a (Å)	Band gap E_g (eV)	Crystal Structure
$CsPbF_3$	Calc. Theo. Exp.	4.973 4.77 [59], 4.79 [60] 4.79 [61]	2.987 3.92 [59], 2.642 [8]	Cubic
$CsPbCl_3$	Calc. Theo. Exp.	5.86 5.78 [62] 5.62 [23]	2.218 2.168 [23] 2.93 [63], 2.27 [64]	Cubic
$CsPbBr_3$	Calc. Theo. Exp.	6.138 6.005 [23], 6.01, [65], 5.99 [22] 5.87 [66]	1.900 1.61 [23], 1.76 [65], 1.66 [22] 2.3 [67]	Cubic
$CsPbI_3$	Calc. Theo. Exp.	6.515 6.26 [68], 6.401 [69] 6.28 [70], 6.017 [71]	1.516 1.34 [68], 1.56 [69] 1.73 [70], 1.73 [71]	Cubic

3.2. Mechanical properties

To determine the mechanical properties of the cube crystals of $CsPbX_3$, three different elastic constants C_{11}, C_{12}, and C_{44} were chosen [72], [73]. For these crystals, the Born criteria were used to justify mechanical stability, and it is evident that all of them are mechanically stable because they all meet the specifications [74], and the following relations are fulfilled for a material to be cubically stable,

$$C_{11}–C_{12} > 0;\quad C_{11} > 0;\qquad C_{44} > 0;\ C_{11} + 2C_{12} > 0;\quad C_{12} < B < C_{11}.$$

Fig. 3(a) shows the relationship between the compound $CsPbX_3$ and the elastic constants. C_{11}, C_{12}, and C_{44} reach their maximum values for $CsPbF_3$. The mechanical parameters can be measured using the following formulas [75]–[77]:

$$G_V = \frac{1}{5}(3C_{44} + C_{11} - C_{12}),\ G_R = \frac{5(C_{11}-C_{12})C_{44}}{3(C_{11}-C_{12})+4C_{44}},\ B_V = B_R = \frac{C_{11}+2C_{12}}{3} \quad (1)$$

To calculate the bulk and shear and Young's moduli, the Reuss and Voigt approximations must be used. G_V, G_R, B_V and B_R are used to find the shear, Bulk, and Young's moduli as

$$G = \frac{G_V+G_R}{2},\ B = \frac{B_V+B_R}{2},\ E = \frac{9GB}{3B+G} \quad (2)$$

For Poisson's ratio and Cauchy's pressure, the expressions used are

$$v = \frac{3B - 2G}{2(3B+G)}, P_C = C_{12} - C_{44.} \quad (3)$$

We obtained data for many ratios, which are depicted in Fig. 3(b–d), to determine the mechanical features of the chosen materials. In Fig. 3(b), the decreasing trend in values for Young's modulus (E) [78], bulk modulus (B) [79], and shear modulus (G) [80] is evident for all materials $CsPbF_3$ > $CsPbI_3$ > $CsPbCl_3$ > $CsPbBr_3$. This result shows that $CsPbF_3$ is the stiffest among all other perovskites when the tensile, volumetric, and shear stresses are applied and exhibit high resistance within elastic deformation. The bulk modulus to the shear modulus ratio is known as Pugh's ratio (B/G). Pugh proposes the use of an elastic modulus B/G to characterize a material's plastic qualities (ductility and brittleness). If the Pugh's ratio is higher than 1.75, the material is brittle [81]. Our selected materials, $CsPbX_3$ (X=Cl, Br, F, I) demonstrated ductile behaviour at 0 GPa shown in Fig. 3(c). The maximum Pugh's ratio was found for $CsPbBr_3$ while the lowest was found in $CsPbF_3$. It means among the selected materials $CsPbBr_3$ is the most ductile. The decreasing trend in materials can be seen as $CsPbBr_3$ > $CsPbCl_3$ > $CsPbI_3$ > $CsPbF_3$.

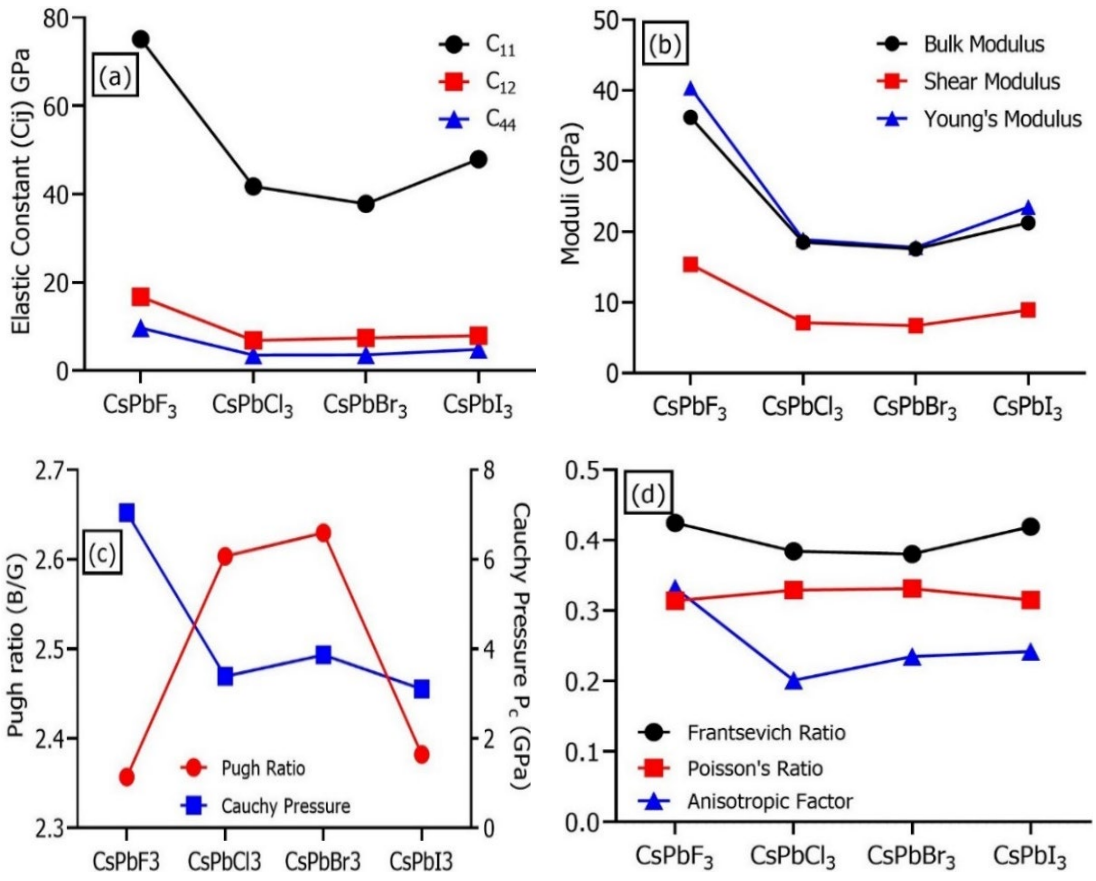

Fig. 3. Variation in (a) Elastic Constants, (b) Elastic moduli, (c) Pugh ratio and Cauchy Pressure, (d) Frantsevich ratio, Poisson ratio, and Anisotropic factor for $CsPbF_3$, $CsPbCl_3$, $CsPbBr_3$ and $CsPbI_3$.

An additional parameter for ductile and brittle behaviour is Cauchy pressure (P_C), which is seen in Fig. 3(c). If the Cauchy pressure (P_C) is positive, the material will be ductile; if the P_C is negative, the material will be brittle [82]. According to the projected DFT results, all of the chosen materials that are ductile at 0 GPa have a positive Cauchy pressure (P_C). The decreasing trend in

Cauchy's pressure in our estimated simulation results is $CsPbF_3$ > $CsPbBr_3$ > $CsPbCl_3$ > $CsPbI_3$. The Frantsevich ratio represents the ratio between the bulk and shear moduli [83]. If the Frantsevich ratio is less than 0.57, the material will be ductile; if it is more than 0.57, it will be brittle. In our approximated simulation findings, all selected materials showed a ductile nature, and the maximum value of the Frantsevich ratio was found in $CsPbF_3$ and minimum in $CsPbBr_3$ shown in Fig. 3(d). Poisson's ratio (υ) is another important mechanical component that determines a material's brittleness or ductility; a value of υ less than 0.26 suggests brittle behavior or ionic bonding, whereas a value more than 0.26 shows ductile behavior or covalent bonding [84], [85]. Fig. 3(d) shows the values of Poisson's ratio for all selected materials. The highest value of ductility was found for $CsPbBr_3$. If the material properties vary with the variation in crystallographic orientation, then the material is anisotropic. The anisotropic factor can be calculated as $A = \frac{2C_{44}}{C_{11} - C_{12}}$ [86], [87]. For all selected materials $CsPbX_3$ the result is found anisotropic shown in Fig. 3(d). For all the materials chosen, the anisotropy is determined to be $CsPbF_3$ > $CsPbI_3$ > $CsPbBr_3$ > $CsPbCl_3$, in decreasing order.

Table 2. Values of Elastic constants (C_{11}, C_{12}, C_{44}), Elastic Moduli (Bulk B, Shear G, Young Y), Pugh's ratio B/G, Poisson Ratio (υ).

$CsPbX_3$		**C_{11}**	**C_{12}**	**C_{44}**	**B**	**G**	**Y**	**B/G**	**υ**
	Present	75.12	16.72	9.68	36.19	15.35	40.36	2.35	
$CsPbF_3$	work	97.91	20.36	6.33	26.50	13.53	34.83	2.00	0.31
	Ref.	[59]	[59]	[59]	[59]	[59]	[59]	[59]	
	Present	41.76	6.88	3.50	18.51	7.11	18.91	2.60	0.32
$CsPbCl_3$	work	48.35	7.881	4.92	21.37	9.05	23.79	2.361	0.31
	Ref.	[62]	[62]	[62]	[62]	[62]	[62]	[62]	[62]
	Present	37.77	7.42	3.56	17.54	6.67	17.76	2.63	0.33
$CsPbBr_3$	work	44.93	6.93	4.47	28.30	7.82	21.47	3.619	0.37
	Ref.	[88]	[88]	[88]	[62]	[62]	[62]	[62]	[62]
	Present	47.90	7.94	4.84	21.26	8.92	23.49	2.38	0.31
$CsPbI_3$	work	34.40	4.71	3.84	14.61	6.85	17.79	2.06	0.29
	Ref.	[69]	[69]	[69]	[69]	[69]	[69]	[62]	[69]

3.3. Electronic properties

The energy band diagram featuring the Brillouin zone k-points in the sample depicts band gap energy. Electronic band structures of $CsPbX_3$ are displayed in Fig. 4(a–d). The power differences between the top (VB) and bottom (CB) of the valence band and the conduction band produce the band gap. In our calculated result the highest value of the band gap is 2.987 eV for $CsPbF_3$. In all other materials, the band decreased up to 26% in $CsPbCl_3$, 36% in $CsPbBr_3$, and 49% in $CsPbI_3$ from the calculated value of $CsPbF_3$. The ideal range for the perovskites-based solar cells is from 1.2 eV to 1.8 eV and the best energy band gap range is found for $CsPbI_3$. One can readily see from Fig. 4(a–d) that there is a direct band gap for $CsPbF_3$ and $CsPbCl_3$ at Z-zone while for $CsPbBr_3$ and $CsPbI_3$ at G-zone. As the phonon contributions to pair production are limited, electron transfer in the direct band gap material gives minimal momentum loss for carrier propagation. The top of the VB is clearly shown to be more well dispersed than the bottom of the CB in Fig. 4(b–d), indicating that the photo-generated holes have a lesser mass. Higher carrier mobility is correlated with a lower carrier effective mass. Another factor which can be seen in Fig. 4(a–d) is that the number of energy states and expansion of energy states is formed in the increasing order for $CsPbF_3$ < $CsPbCl_3$ < $CsPbBr_3$ < $CsPbI_3$. The best option for perovskite solar cells is $CsPbI_3$, according to our DFT results for band gap.

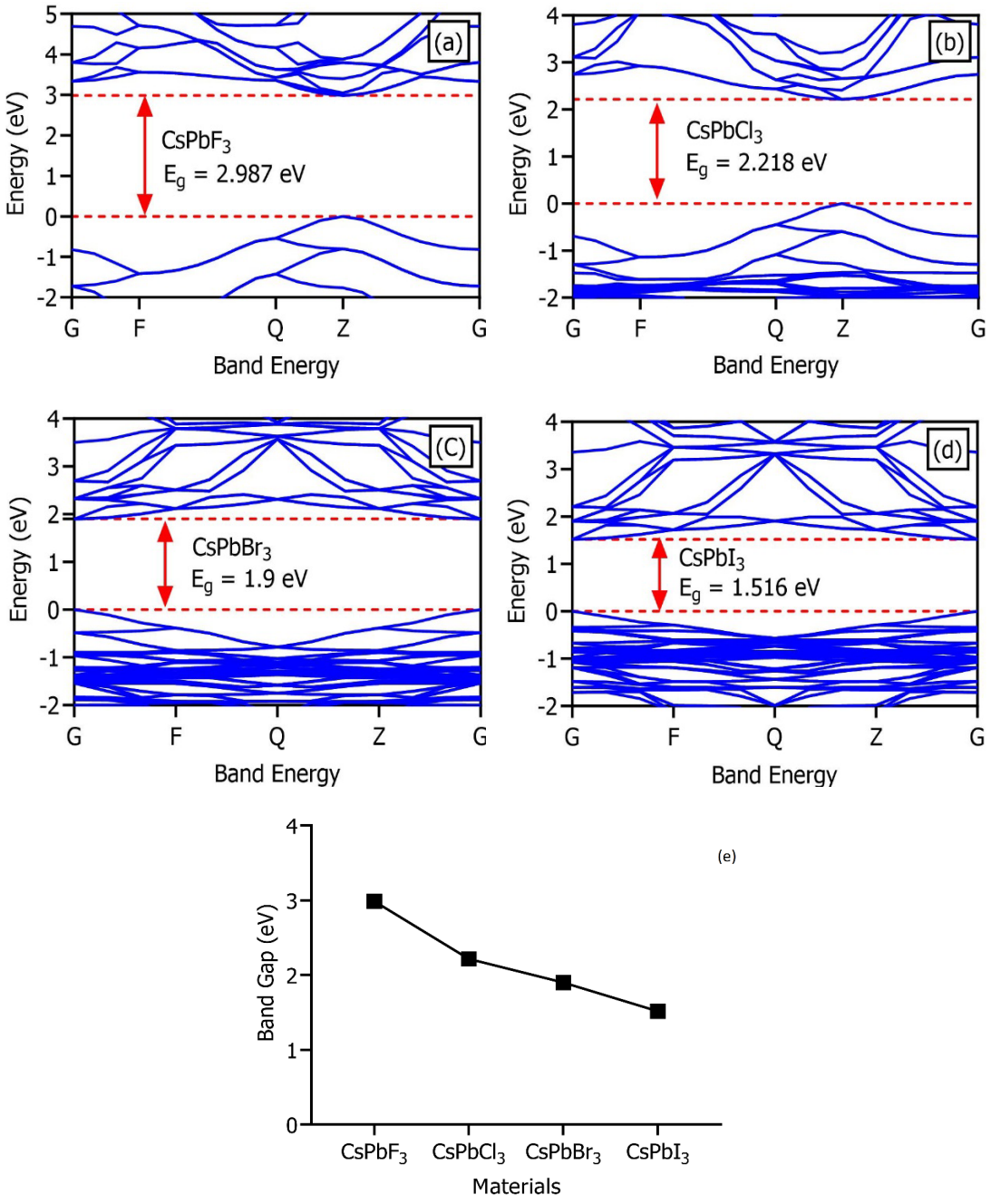

Fig. 4. Band structure of (a) $CsPbF_3$, (b) $CsPbCl_3$, (c) $CsPbBr_3$, and (d) $CsPbI_3$ at 0 GPa (e) Band gaps.

Details regarding compounds $CsPbX_3$'s partial density of states (PDOS) are provided in Fig. 5. Fig. 5(a) makes this very evident: for $CsPbX_3$ (Br, I), s-states contribute significantly to the lower valence band and an intermediate amount to the upper valence band. In a similar vein, they play a considerable role in the development of the lower conduction band. A small amount of s-states contributes to the production of the top and bottom valence bands and a little amount to the development of the top and lower conduction bands in $CsPbCl_3$. The contribution of s-states in the $CsPbF_3$ instance is primarily observed in the lower valence band, with a smaller contribution in the bottom conduction band. Fig. 5(b) shows all of the combinations $CsPbX_3$ (X = F, Cl, Br, I), where the top valence band represents the contribution of the p-states and the lower conduction band represents the intermediate contribution. As seen in Fig. 5(c), d-states play no discernible function in the top valence band or any kind of conduction band. The graph of the total density of states

TDOS shown in Fig. 6 represents expansion in valence and conduction bands. The maximum expansion in the valence band is found in $CsPbF_3$ and the conduction band for $CsPbBr_3$.

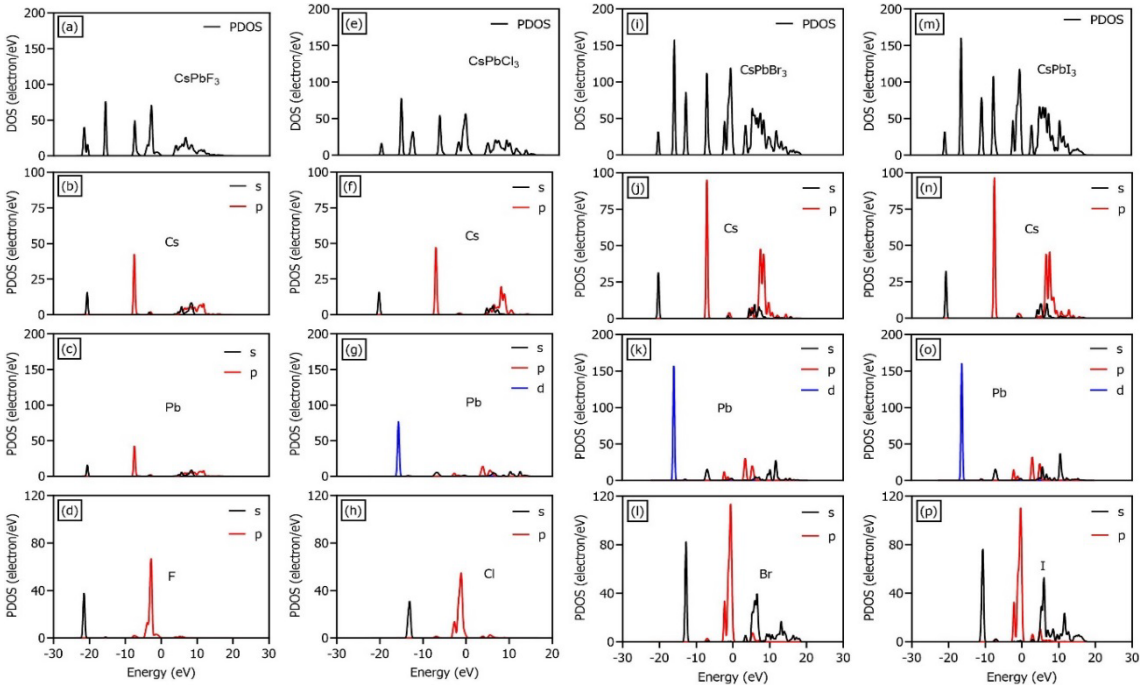

Fig. 5. Partial density of states (PDOS) for $CsPbF_3$, $CsPbCl_3$, $CsPbBr_3$, and $CsPbI_3$.

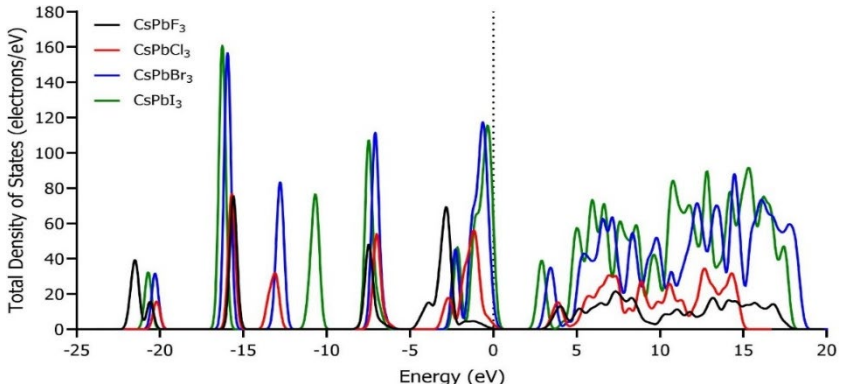

Fig. 6. The total density of states (TDOS) for $CsPbX_3$.

3.4. Optical properties

The photonic exchanges of the material can reveal evidence of the characteristics and forecast the behavior of the material when external electromagnetic waves are induced [89]. According to the materials' optical spectra, these characteristics are examined for electron conduction empty and filled states, the structure of the band, types of bonds, and material internal structures. The estimated computational calculations are performed for analyzing the optical properties of $CsPbX_3$ including the absorption $I(\omega)$, real and imaginary conductivities $\sigma_1(\omega)$ & $\sigma_2(\omega)$, real and imaginary dielectric functions $\varepsilon_1(\omega)$ and $\varepsilon_2(\omega)$, energy loss function $L(\omega)$, reflectivity $R(\omega)$ and refractive indices real $n_1(\omega)$ and imaginary $n_2(\omega)$. The key fundamental equations presented in Table III were utilized to calculate each of the attributes listed earlier [90], [91].

Table 3. Set of equations used to calculate optical parameters.

Optical Parameter	Equation
Absorption coefficient	$I(\omega) = \sqrt{2}\omega\left(\sqrt{\varepsilon_1(\omega)^2 + \varepsilon_2(\omega)^2} - \varepsilon_1(\omega)\right)^{\frac{1}{2}}$
Extinction coefficient	$K(\omega) = \frac{I(\omega)}{2\omega}$
Energy loss function	$L(\omega) = \frac{\varepsilon}{(\varepsilon_1(\omega)^2 + \varepsilon_2(\omega)^2)}$
Refractive index	$n(\omega) = \left(\frac{1}{\sqrt{2}}\right)\left(\sqrt{\varepsilon_1(\omega)^2 + \varepsilon_2(\omega)^2} - \varepsilon_1(\omega)\right)^{\frac{1}{2}}$
Reflectivity coefficient	$r(\omega) = \frac{n + iK - 1}{n + iK + 1}$
Dielectric function $\boldsymbol{\varepsilon_1(\omega)}$: Real part $\boldsymbol{\varepsilon_2(\omega)}$: Imaginary part	$\sqrt{\varepsilon(\omega)} = N(\omega) = n(\omega) + iK(\omega)$ $\varepsilon_1(\omega) = n^2 - K^2, \quad \varepsilon_2(\omega) = 2nK$ $\varepsilon(\omega) = \varepsilon_1(\omega) + i\varepsilon_2(\omega)$ [49], [50]
Conductivity	$\sigma = \sigma_1 + i\sigma_2 = -i\frac{\omega}{4\pi}(\varepsilon - 1)$

Fig. 7(a) illustrates how the optical absorbance of $CsPbX_3$ perovskites varies with the increase in incident electromagnetic wave frequency. As compared to Br, F, and l-based perovskites, the value of absorption for the CI-based perovskite shows that it is most intense in the ultraviolet range. The optical band gaps are as E_g ($CsPbF_3$) > E_g ($CsPbCl_3$) > E_g ($CsPbBr_3$) > E_g ($CsPbI_3$) from the absorption peaks of matching materials, which is consistent with the estimated values of E_g of $CsPbX_3$ perovskites. The maximum intensity of the highest absorption peaks can be seen between 14 – 17 eV approximately. According to the DFT absorption rate the highest absorption or penetration of radiation is seen in $CsPbCl_3$ and $CsPbF_3$ which could be the best option for scintillators. The lowest absorption wave capability is found in $CsPbI_3$ as can be seen in Fig. 7(a) the edge length of the absorption graph. It could be the best choice for solar cell and photodiode applications.

Fig. 7(b) represents the real and imaginary photo conductivities of estimated computational results for $CsPbX_3$ as a function of wave frequency. These materials' photoconductivity comparisons reveal some peaks across a variety of energy spectrums. The first peaks of conductivity in $CsPbX_3$ are orderly in terms of the energy as $\sigma(CsPbI_3) > \sigma(CsPbBr_3) > \sigma(CsPbCl_3) > \sigma(CsPbF_3)$. The imaginary component of the conductivity may be used to describe the level of charge slowness needed to respond to changes in the electric field. The real dielectric constant is a measure of how much electrical energy a material can hold in an electric field. It is a dimensionless quantity that can be computed as the distinction between the density of the electric flux in a material under constant electric field application and the electric flux density in a vacuum. The real and imaginary dielectric constant values with the variation in the frequency of electromagnetic waves are revealed in Fig. 7(c). One can readily see here the highest to lowest pattern in dielectric for our results is $\varepsilon_1(\omega)$ ($CsPbI_3$) > $\varepsilon_1(\omega)$ ($CsPbBr_3$) > $\varepsilon_1(\omega)$ ($CsPbCl_3$) > $\varepsilon_1(\omega)$ ($CsPbF_3$). The highest ability to store electric energy is found in $CsPbI_3$.

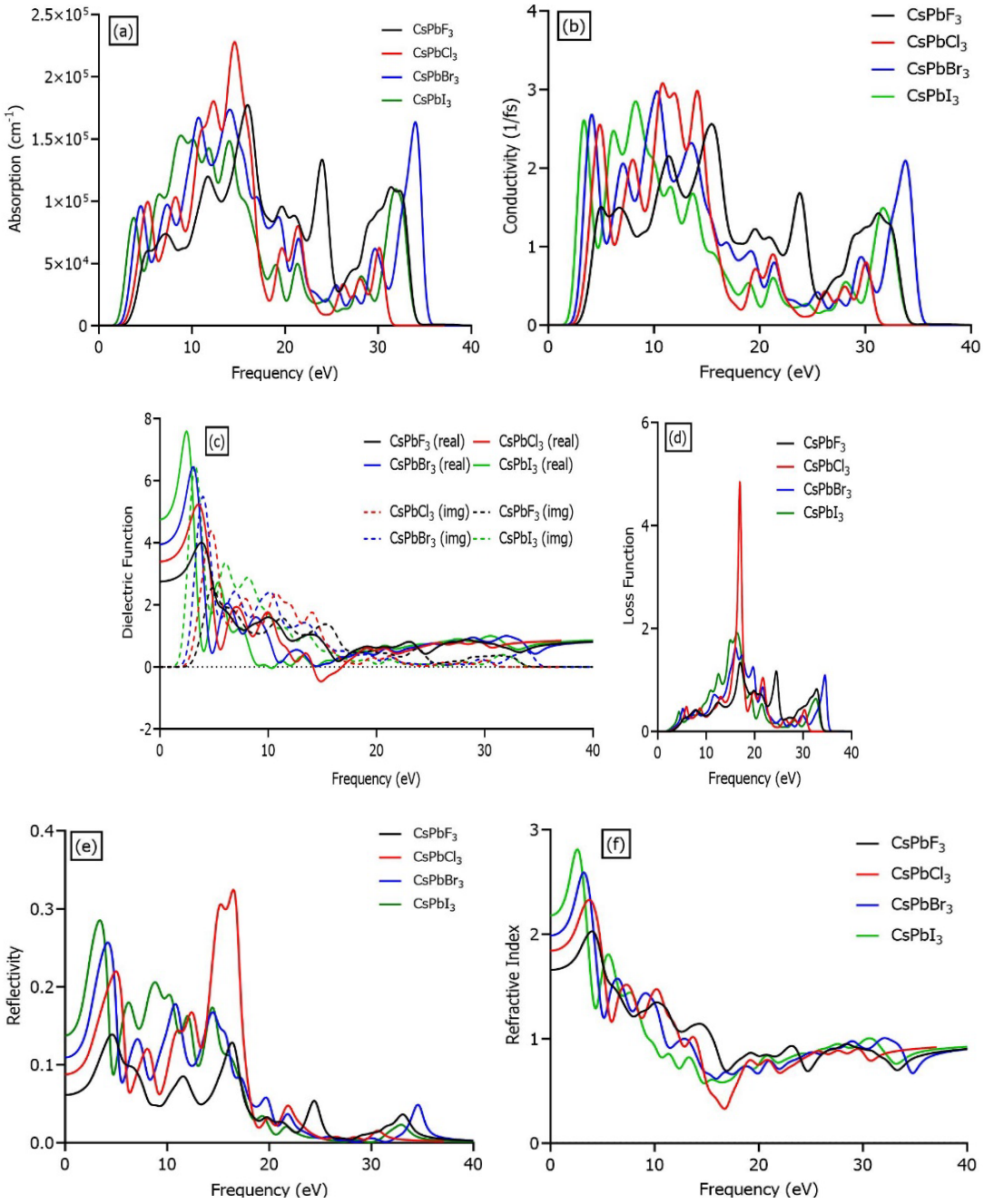

Fig. 7. (a) Absorption, (b) conductivity, (c) dielectric function, (d) energy loss function, (e) reflectivity, and (f) refractive index for $CsPbX_3$.

When electromagnetic radiations are impacted upon a medium, the energy loss function (ELF) describes how much energy is lost within the material. In this scenario, we assume that the electrons oscillate in plasma rather than being fixed to their lattice positions. These oscillations correlate to the ELF's maximum value. From Fig. 7(d) one can readily see where the maximum value of the loss function is found for $CsPbCl_3$. For optoelectronic applications, reflectivity is a vital optical property that defines the surface nature of the materials. The reflectivity spectra of $CsPbX_3$ perovskites are shown in Fig. 7(e). It is noticeable from these results that all the examined cubic perovskite compounds have very low reflectivity; nevertheless, at the optical range, the reflectivity is highest for $CsPbI_3$ and lowest for $CsPbCl_3$ perovskites at the lowest frequency of electromagnetic waves. From 14 – 19 eV the maximum reflectivity was found for $CsPbCl_3$. Excitonic resonances in the electronic structure of $CsPbCl_3$ are responsible for the reflectivity peak

at 14–19 eV. When a photon is absorbed by a substance and an electron-hole pair is produced, the result is an exciton, a bound state comprising an electron and a hole. The link between the valence and the conduction band in $CsPbCl_3$ results in excitonic resonances. These resonances can enhance the absorption of light in the UV range as shown in Fig. 7(a), leading to a corresponding increase in reflectivity in Fig. 7(e).

The refractive index is a property that describes how much light is bent when it passes through a material in the perspective of DFT. The dielectric function, which explains how a material reacts to an outside electric field, is connected to the refractive index. The refractive index affects the real portion of the dielectric function and controls how fast light travels through a substance. By computing the real component of the dielectric function and utilizing it to derive the index of refraction, the real part of the dielectric function can be used to calculate the refractive index of a material. The refractive index is a significant factor in the construction of optical devices including lenses, prisms, and waveguides, and is an important statistic for interpreting the optical properties of materials. DFT estimated calculations to predict the refractive index of $CsPbX_3$ can be seen in Fig. 7(f).

4. Conclusions

The suitability of perovskite materials $CsPbX_3$ for photodetector and solar cell systems was evaluated by investigating their simulated electronic, structural, and optical properties. The highest lattice constant and volume were found in $CsPbI_3$ among the $CsPbX_3$ perovskites. The simulated results showed a decreasing trend in the values of Young's (E), bulk (B), and shear (G) moduli in the order of $CsPbF_3$ > $CsPbl_3$ > $CsPbCl_3$ > $CsPbBr_3$. $CsPbF_3$ was found to be the stiffest material. According to our calculations, $CsPbF_3$ had the largest band gap of 2.987 eV, while the band gaps of all other materials were reduced from the estimated value of $CsPbF_3$ by up to 26% in $CsPbCl_3$, 36% in $CsPbBr_3$, and 49% in $CsPbI_3$.

The absorption value of the Cl-based perovskite was found to be the most intense in the ultraviolet (UV) region when matched with Br, F, and I-based perovskites. In our results, $CsPbI_3$ seemed to have the largest dielectric constant or capacity to store electric energy. The maximum value of the loss function was found for $CsPbCl_3$. The reflectivity was found to be highest for $CsPbI_3$ and lowest for $CsPbCl_3$ perovskites. From the calculated band gap, optical, and mechanical characteristics of $CsPbX_3$, it can be concluded that $CsPbI_3$ and $CsPbBr_3$ are the best choices for the manufacturing of solar cells, LEDs, and photodiodes, while $CsPbCl_3$ and $CsPbF_3$ are good choices for perovskite scintillators.

Acknowledgments

The authors would like to acknowledge the Deanship of Graduate Studies and Scientific Research, Taif University for funding this work.

References

[1] L. Liang et al., Adv Mater Technol, vol. 8, no. 3, p. 2200419, Feb. 2023; https://doi.org/10.1002/admt.202200419

[2] A. Najim et al., Mater Sci Semicond Process, vol. 141, Apr. 2022; https://doi.org/10.1016/j.mssp.2021.106442

[3] M. R. Islam, B. K. Moghal, R. Moshwan, M. R. Islam, B. K. Moghal, R. Moshwan, PhyS, vol. 97, no. 6, p. 065704, Jun. 2022; https://doi.org/10.1088/1402-4896/ac6e9a

[4] Y. Nassah et al., Bulletin of Materials Science, vol. 46, no. 2, Jun. 2023; https://doi.org/10.1007/s12034-023-02890-x

[5] S. Lim, S. Han, D. Kim, J. Min, J. Choi, T. Park, Adv Mater, vol. 35, no. 4, Jan. 2023;

https://doi.org/10.1002/adma.202203430
[6] P. M. Maleka et al., PhyS, vol. 98, no. 4, p. 045505, Apr. 2023; https://doi.org/10.1088/1402-4896/acbf88
[7] M. J. Patel, S. K. Gupta, P. N. Gajjar, M. J. Patel, S. K. Gupta, P. N. Gajjar, JPCS, vol. 176, p. 111264, May 2023; https://doi.org/10.1016/j.jpcs.2023.111264
[8] A. Amudhavalli, R. Rajeswarapalanichamy, R. Padmavathy, K. Iyakutti, Acta Physica Polonica A vol. 139, no. 6, 2021; https://doi.org/10.12693/APhysPolA.139.692
[9] D. Jayan K, V. Sebastian, J. Kurian, Solar Energy, vol. 221, pp. 99-108, Jun. 2021; https://doi.org/10.1016/j.solener.2021.04.030
[10] P. Su, Y. Huang, Y. Li, C. Hu, W. Shi, Surfaces and Interfaces, vol. 37, p. 102719, Apr. 2023; https://doi.org/10.1016/j.surfin.2023.102719
[11] N. Zhang, Q. Na, Q. Xie, S. Jia, Crystals 2022, Vol. 12, Page 1274, vol. 12, no. 9, p. 1274, Sep. 2022; https://doi.org/10.3390/cryst12091274
[12] D. Wu et al., Advanced Devices & Instrumentation, vol. 4, Feb. 2023; https://doi.org/10.34133/adi.0006
[13] Z. Jia et al., Mater Adv, vol. 4, no. 1, pp. 79-104, Jan. 2023; https://doi.org/10.1039/D2MA00779G
[14] H. Bu et al., Adv Electron Mater, vol. 8, no. 5, May 2022; https://doi.org/10.1002/aelm.202101204
[15] A. A. Asif, R. Singh, G. F. Alapatt, Journal of Renewable and Sustainable Energy, vol. 7, no. 4, p. 43120, Jul. 2015; https://doi.org/10.1063/1.4927329
[16] R. Sharma et al., SoEn, vol. 244, pp. 516-535, Sep. 2022; https://doi.org/10.1016/j.solener.2022.08.001
[17] F. Elfatouaki, O. Farkad, E. A. Ibnouelghazi, D. Abouelaoualim, A. Outzourhit, Mater Sci Semicond Process, vol. 143, p. 106488, Jun. 2022; https://doi.org/10.1016/j.mssp.2022.106488
[18] Y. Yin, Y. Zhou, M. H. Rafailovich, C. Y. Nam, Nanotechnology, vol. 34, no. 17, Apr. 2023; https://doi.org/10.1088/1361-6528/acb441
[19] J. T. Dubose, P. V. Kamat, Chem Rev, vol. 122, no. 15, pp. 12475-12494, Aug. 2022; https://doi.org/10.1021/acs.chemrev.2c00172
[20] N. H. Mohd Kaus, M. L. Ibrahim, S. S. Imam, S. I. S. Mashuri, Y. Kumar, Efficient Visible-Light-Driven Perovskites Photocatalysis: Design, Modification and Application, pp. 357-398, 2022; https://doi.org/10.1007/978-3-030-77371-7_13
[21] W. Xiang, W. Tress, Advanced Materials, vol. 31, no. 44, p. 1902851, Nov. 2019; https://doi.org/10.1002/adma.201902851
[22] R. Rajeswarapalanichamy, A. Amudhavalli, R. Padmavathy, K. Iyakutti, Materials Science and Engineering: B, vol. 258, p. 114560, Aug. 2020; https://doi.org/10.1016/j.mseb.2020.114560
[23] M. Maqbool et al., J Alloys Compd, vol. 705, pp. 828-839, May 2017; https://doi.org/10.1016/j.jallcom.2017.02.147
[24] F. Haque et al., ACS Omega, vol. 3, no. 9, pp. 11937-11944, Sep. 2018; https://doi.org/10.1021/acsomega.8b01589
[25] S. L. Hamukwaya et al., Coatings 2022, Vol. 12, Page 252, vol. 12, no. 2, p. 252, Feb. 2022; https://doi.org/10.3390/coatings12020252
[26] S. Ma, G. Yuan, Y. Zhang, N. Yang, Y. Li, Q. Chen, Energy Environ Sci, vol. 15, no. 1, pp. 13-55, Jan. 2022; https://doi.org/10.1039/D1EE02882K
[27] W. J. Yin, J. H. Yang, J. Kang, Y. Yan, S. H. Wei, J Mater Chem A Mater, vol. 3, no. 17, pp. 8926-8942, Apr. 2015; https://doi.org/10.1039/C4TA05033A
[28] H. Chen, M. Li, B. Wang, S. Ming, J. Su, J Alloys Compd, vol. 862, p. 158442, May 2021; https://doi.org/10.1016/j.jallcom.2020.158442
[29] J. Ma et al., Matter, vol. 4, no. 1, pp. 313-327, Jan. 2021; https://doi.org/10.1016/j.matt.2020.10.023
[30] M. Hussain, M. Rashid, A. Ali, M. F. Bhopal, A. S. Bhatti, Ceram Int, vol. 46, no. 13, pp.

21378-21387, Sep. 2020; https://doi.org/10.1016/j.ceramint.2020.05.235
[31] Y. Zhou, J. Chen, O. M. Bakr, O. F. Mohammed, ACS Energy Lett, vol. 6, no. 2, pp. 739-768, Feb. 2021; https://doi.org/10.1021/acsenergylett.0c02430
[32] C. Wang et al., J Eur Ceram Soc, vol. 40, no. 5, pp. 2234-2238, May 2020; https://doi.org/10.1016/j.jeurceramsoc.2020.01.016
[33] M. Zhang et al., Physical Chemistry Chemical Physics, vol. 25, no. 13, pp. 9592-9598, Mar. 2023; https://doi.org/10.1039/D2CP05867G
[34] L. Lu, M. Sun, T. Wu, Q. Lu, B. Chen, B. Huang, Nanoscale Adv, vol. 4, no. 3, pp. 680-696, Feb. 2022; https://doi.org/10.1039/D1NA00815C
[35] H. Milani Moghaddam, M. Fallah, Journal of Acoustical Society of Iran, vol. 8, no. 1, pp. 68-77, 2020, Accessed: Apr. 20, 2023.
[36] V. B. Mykhaylyk et al., J Mater Chem C Mater, vol. 11, no. 2, pp. 656-665, Jan. 2023; https://doi.org/10.1039/D2TC04631H
[37] N. A. Abdulkareem, S. A. Sami, B. H. Elias, Science Journal of University of Zakho, vol. 8, no. 1, pp. 23-28, Mar. 2020; https://doi.org/10.25271/sjuoz.2020.8.1.632
[38] J. Liang, J. Liu, Z. Jin, Solar RRL, vol. 1, no. 10, Oct. 2017; https://doi.org/10.1002/solr.201700086
[39] N. Pandey, S. Chakrabarti, N. Pandey, S. Chakrabarti, SPIE, vol. 12150, p. 1215008, Apr. 2022; https://doi.org/10.1117/12.2620027
[40] N. Pandey, A. Kumar, S. Chakrabarti, RSC Adv, vol. 9, no. 51, pp. 29556-29565, Sep. 2019; https://doi.org/10.1039/C9RA05685H
[41] P. Ramasamy, D. H. Lim, B. Kim, S. H. Lee, M. S. Lee, J. S. Lee, Chemical Communications, vol. 52, no. 10, pp. 2067-2070, Jan. 2016; https://doi.org/10.1039/C5CC08643D
[42] M. Ahmadi, T. Wu, B. Hu, Adv Mater, vol. 29, no. 41, Nov. 2017; https://doi.org/10.1002/adma.201605242
[43] X. Wang, M. Li, B. Zhang, H. Wang, Y. Zhao, B. Wang, Org Electron, vol. 52, pp. 172-183, Jan. 2018; https://doi.org/10.1016/j.orgel.2017.10.027
[44] M. Gong et al., ACS Nano, vol. 13, no. 2, pp. 1772-1783, Feb. 2019; https://doi.org/10.1021/acsnano.8b07850
[45] H. Hu, Z. Han, B. Huang, Y. Dong, Y. Zou, J Colloid Interface Sci, vol. 554, pp. 619-626, Oct. 2019; https://doi.org/10.1016/j.jcis.2019.07.044
[46] D. Ren et al., Journal of Physical Chemistry Letters, vol. 13, no. 1, pp. 267-273, Jan. 2022; https://doi.org/10.1021/acs.jpclett.1c03891
[47] X. Zhang et al., J Mater Chem C Mater, vol. 10, no. 40, pp. 14892-14904, Oct. 2022; https://doi.org/10.1039/D2TC02846H
[48] A. Mandal, A. Ghosh, D. Ghosh, S. Bhattacharyya, ACS Appl Mater Interfaces, vol. 13, no. 36, 2021; https://doi.org/10.1021/acsami.1c13452
[49] L. Q. Jiang et al., JPCS, vol. 67, no. 7, pp. 1531-1536, Jul. 2006; https://doi.org/10.1016/j.jpcs.2006.02.004
[50] M. Rizwan et al., InJPh, vol. 96, no. 4, pp. 1-9, Mar. 2022; https://doi.org/10.1007/s12648-021-02031-2
[51] M. Rizwan et al., PhSS, vol. 63, no. 1, pp. 134-140, Jan. 2021; https://doi.org/10.1134/S1063783421010182
[52] G. Murtaza, Hayatullah, R. Khenata, M. N. Khalid, S. Naeem, Physica B Condens Matter, vol. 410, no. 1, pp. 131-136, Feb. 2013; https://doi.org/10.1016/j.physb.2012.10.024
[53] J. P. Perdew et al., Phys Rev B Condens Matter, vol. 46, no. 11, pp. 6671-6687, 1992; https://doi.org/10.1103/PhysRevB.46.6671
[54] J. P. Perdew, K. Burke, M. Ernzerhof, Phys Rev Lett, vol. 77, no. 18, p. 3865, Oct. 1996; https://doi.org/10.1103/PhysRevLett.77.3865
[55] C. Dotzler, G. V. M. Williams, A. Edgar, Current Applied Physics, vol. 8, no. 3-4, pp. 447-450, May 2008; https://doi.org/10.1016/j.cap.2007.10.078

[56] W. Kohn, Rev Mod Phys, vol. 71, no. 5, p. 1253, Oct. 1999; https://doi.org/10.1103/RevModPhys.71.1253
[57] P. Hohenberg W. Kohn, Physical Review, vol. 136, no. 3B, p. B864, Nov. 1964; https://doi.org/10.1103/PhysRev.136.B864
[58] W. Kohn, L. J. Sham, Physical Review, vol. 140, no. 4A, p. A1133, Nov. 1965; https://doi.org/10.1103/PhysRev.140.A1133
[59] Q. Mahmood et al., PhyB, vol. 571, pp. 87-92, Oct. 2019; https://doi.org/10.1016/j.physb.2019.06.061
[60] G. Murtaza, I. Ahmad, M. Maqbool, H. A. R. Aliabad, A. Afaq, ChPhL, vol. 28, no. 11, p. 117803, 2011; https://doi.org/10.1088/0256-307X/28/11/117803
[61] P. Berastegui, S. Hull, S. G. Eriksson, Journal of Physics: Condensed Matter, vol. 13, no. 22, p. 5077, Jun. 2001; https://doi.org/10.1088/0953-8984/13/22/305
[62] M. Aktary, M. Kamruzzaman, R. Afrose, RSC Adv, vol. 12, no. 36, pp. 23704-23717, Aug. 2022; https://doi.org/10.1039/D2RA04591E
[63] T. Liu, S. Salek, J. C. Byers, Electrochem commun, vol. 143, p. 107381, Oct. 2022; https://doi.org/10.1016/j.elecom.2022.107381
[64] L. Zhang, L. Wang, K. Wang, B. Zou, Journal of Physical Chemistry C, vol. 122, no. 27, pp. 15220-15225, Jul. 2018; https://doi.org/10.1021/acs.jpcc.8b05397
[65] Y. Ye et al., Chinese Physics B, vol. 24, no. 11, pp. 116302-116302, Nov. 2015; https://doi.org/10.1088/1674-1056/24/11/116302
[66] D. M. Trots, S. V. Myagkota, Journal of Physics and Chemistry of Solids, vol. 69, no. 10, pp. 2520-2526, Oct. 2008; https://doi.org/10.1016/j.jpcs.2008.05.007
[67] F. Hao, C. C. Stoumpos, R. P. H. Chang, M. G. Kanatzidis, J Am Chem Soc, vol. 136, no. 22, pp. 8094-8099, Jun. 2014; https://doi.org/10.1021/ja5033259
[68] S. Idrissi, H. Labrim, L. Bahmad, A. Benyoussef, Chem Phys Lett, vol. 766, p. 138347, Mar. 2021; https://doi.org/10.1016/j.cplett.2021.138347
[69] M. Afsari, A. Boochani, M. Hantezadeh, Optik (Stuttg), vol. 127, no. 23, pp. 11433-11443, Dec. 2016; https://doi.org/10.1016/j.ijleo.2016.09.013
[70] M. R. Filip, G. E. Eperon, H. J. Snaith, F. Giustino, Nature Communications 2014 5:1, vol. 5, no. 1, pp. 1-9, Dec. 2014; https://doi.org/10.1038/ncomms6757
[71] G. E. Eperon, S. D. Stranks, C. Menelaou, M. B. Johnston, L. M. Herz, H. J. Snaith, Energy Environ Sci, vol. 7, no. 3, pp. 982-988, Feb. 2014; https://doi.org/10.1039/c3ee43822h
[72] J. Chen, X. Zhang, L. Yang, F. Wang, Commun Theor Phys, vol. 73, no. 4, p. 045702, Mar. 2021; https://doi.org/10.1088/1572-9494/abe367
[73] M. A. Rashid et al., First-principles study of electronic, elastic and optical properties of Zn1-xMgxTe ternary alloys using modified Becke-Johnson potential, 2015; https://doi.org/10.1016/j.mssp.2013.10.031
[74] F. Mouhat, F. X. Coudert, Phys Rev B, vol. 90, no. 22, p. 224104, Dec. 2014; https://doi.org/10.1103/PhysRevB.90.224104
[75] M. Awais, I. Zeba, S. S. A. Gillani, M. Shakil, M. Rizwan, Journal of Physics and Chemistry of Solids, vol. 169, p. 110878, Oct. 2022; https://doi.org/10.1016/j.jpcs.2022.110878
[76] R. Hill, Proceedings of the Physical Society. Section A, vol. 65, no. 5, p. 349, May 1952; https://doi.org/10.1088/0370-1298/65/5/307
[77] G. Vaitheeswaran et al., Phys Rev B Condens Matter Mater Phys, vol. 81, no. 7, Feb. 2010; https://doi.org/10.1103/PhysRevB.81.075105
[78] I. Ilyas et al., JPCS, vol. 165, p. 110642, Jun. 2022; https://doi.org/10.1016/j.jpcs.2022.110642
[79] S. M. J. Zaidi, M. I. Khan, S. S. A. Gillani, M. S. U. Sahar, S. Ullah, M. Tanveer, Mater Res Express, vol. 9, no. 12, p. 125501, Dec. 2022; https://doi.org/10.1088/2053-1591/aca645
[80] A. Gherriche, A. Bouhemadou, Y. Al-Douri, S. Bin-Omran, R. Khenata, M. A. Hadi, Mater Sci Semicond Process, vol. 131, p. 105890, Aug. 2021;

https://doi.org/10.1016/j.mssp.2021.105890
[81] S. F. Pugh, XCII. Relations between the elastic moduli and the plastic properties of polycrystalline pure metals, vol. 45, no. 367, pp. 823-843, Aug. 2009; https://doi.org/10.1080/14786440808520496
[82] S. Ganeshan, S. L. Shang, H. Zhang, Y. Wang, M. Mantina, Z. K. Liu, Intermetallics (Barking), vol. 17, no. 5, pp. 313-318, May 2009; https://doi.org/10.1016/j.intermet.2008.11.005
[83] S. Tariq, A. Ahmed, S. Saad, S. Tariq, AIP Adv, vol. 5, no. 7, p. 077111, Jul. 2015; https://doi.org/10.1063/1.4926437
[84] M. Husain et al., Int J Energy Res, vol. 46, no. 3, pp. 2446-2453, Mar. 2022; https://doi.org/10.1002/er.7319
[85] Y. Benkaddour et al., Journal of Superconductivity and Novel Magnetism 2017 31:2, vol. 31, no. 2, pp. 395-403, Jul. 2017; https://doi.org/10.1007/s10948-017-4234-y
[86] S. Singh et al., Comput Phys Commun, vol. 267, Dec. 2020; https://doi.org/10.1016/j.cpc.2021.108068
[87] A. Moussali, M. B. Amina, B. Fassi, I. Ameri, M. Ameri, Y. Al-Douri, Indian Journal of Physics, vol. 94, no. 11, pp. 1733-1747, Nov. 2020; https://doi.org/10.1007/s12648-019-01627-z
[88] R. I. Maphoto, M. T. Morukuladi, K. T. Malatji, M. C. Masedi, P. E. Ngoepe, JSSST, vol. 11, no. 3, p. 035012, Mar. 2022; https://doi.org/10.1149/2162-8777/ac5eb6
[89] B. Luo, X. Wang, E. Tian, H. Song, G. Li, L. Li, J Alloys Compd, vol. 708, pp. 187-193, Jun. 2017; https://doi.org/10.1016/j.jallcom.2017.02.267
[90] R. A. de Souza, J. Maier, Physical Chemistry Chemical Physics, vol. 5, no. 4, pp. 740-748, Jan. 2003; https://doi.org/10.1039/b209062g
[91] S. Saha, T. P. Sinha, A. Mookerjee, Journal of Physics Condensed Matter, vol. 12, no. 14, pp. 3325-3336, Apr. 2000; https://doi.org/10.1088/0953-8984/12/14/309